OXFORD

ORIGINAL ARTICLE

Impaired mitochondrial dynamics underlie axonal defects in hereditary spastic paraplegias

Kyle Denton[1,†], Yongchao Mou[2,3,†], Chong-Chong Xu[2,3], Dhruvi Shah[2], Jaerak Chang[4,5], Craig Blackstone[4] and Xue-Jun Li[2,3,*]

[1]Department of Neuroscience, University of Connecticut Health Center, Farmington, CT 06030, USA, [2]Department of Biomedical Sciences, University of Illinois College of Medicine at Rockford, Rockford, IL 61107, USA, [3]Department of Bioengineering, University of Illinois at Chicago, Chicago, IL 60607, USA, [4]Cell Biology Section, Neurogenetics Branch, National Institute of Neurological Disorders and Stroke, National Institutes of Health, Bethesda, MD 20892, USA and [5]Departments of Biomedical Science, Brain Science, and Neuroscience Graduate Program, Ajou University School of Medicine, Suwon 443-380, Korea

*To whom correspondence should be addressed at: Department of Biomedical Sciences, University of Illinois College of Medicine at Rockford, Rockford, IL 61107, USA; Department of Bioengineering, University of Illinois at Chicago, Chicago, IL 60607, USA. Tel: +1 8153955882; Fax: +1 8153955666; Email: xjli23@uic.edu

Abstract

Mechanisms by which long corticospinal axons degenerate in hereditary spastic paraplegia (HSP) are largely unknown. Here, we have generated induced pluripotent stem cells (iPSCs) from patients with two autosomal recessive forms of HSP, SPG15 and SPG48, which are caused by mutations in the *ZFYVE26 and AP5Z1* genes encoding proteins in the same complex, the spastizin and AP5Z1 proteins, respectively. In patient iPSC-derived telencephalic glutamatergic and midbrain dopaminergic neurons, neurite number, length and branching are significantly reduced, recapitulating disease-specific phenotypes. We analyzed mitochondrial morphology and noted a significant reduction in both mitochondrial length and their densities within axons of these HSP neurons. Mitochondrial membrane potential was also decreased, confirming functional mitochondrial defects. Notably, mdivi-1, an inhibitor of the mitochondrial fission GTPase DRP1, rescues mitochondrial morphology defects and suppresses the impairment in neurite outgrowth and late-onset apoptosis in HSP neurons. Furthermore, knockdown of these HSP genes causes similar axonal defects, also mitigated by treatment with mdivi-1. Finally, neurite outgrowth defects in SPG15 and SPG48 cortical neurons can be rescued by knocking down DRP1 directly. Thus, abnormal mitochondrial morphology caused by an imbalance of mitochondrial fission and fusion underlies specific axonal defects and serves as a potential therapeutic target for SPG15 and SPG48.

Introduction

Hereditary spastic paraplegias (HSP) are a heterogeneous group of more than 70 genetic disorders that result in progressive lower limb spasticity due to a length-dependent degeneration of corticospinal motor neuron (CSMN) axons (1,2). SPG11 and SPG15 are the most common autosomal recessive HSPs, with strikingly similar clinical phenotypes that comprise thin corpus callosum, cognitive impairment, ataxia, cataracts, retinopathy and early-onset parkinsonism (3,4). SPG11 and SPG15 are caused by biallelic, loss-of-function mutations in the *SPG11* and *ZFYVE26* genes that encode spatacsin and spastizin proteins, respectively (3,5,6). These two proteins are direct binding partners

---

and depend on one another for stability, concordant with the very similar clinical phenotypes observed for SPG11 and SPG15. These proteins localize to a number of regions within cells (7) and have been implicate in endolysosomal functions in particular. They are prevalent in the nervous system (5,7), and their knockdown in zebrafish leads to impaired axonal outgrowth and locomotor impairment, supporting their involvement in axonal development and maintenance (8).

A recent study has shown that both spastizin and spatacsin proteins mediate autophagic lysosome reformation (9), prefiguring a possible mechanism for axonal defects in HSP mediated by impaired lysosomal and autophagic function (9–11). In addition to binding one another, spatacsin and spastizin are responsible for the stability of a common protein complex that also includes the SPG48 protein AP5Z1—the ζ subunit of the heterotetrameric adaptor protein complex-5 (12,13) implicated in endolysosomal dynamics (14,15). As for loss of SPG11 (16) and SPG15 proteins (17), loss of AP5Z1 function in mice leads to accumulation of aberrant endolysosomes (18), supporting a possible pathogenic role for the endolysosomal system in these HSPs.

SPG15 and SPG11 can also present with juvenile-onset parkinsonism, which can improve symptomatically with dopaminergic therapy (19,20). This suggests that in addition to CSMNs, midbrain dopaminergic (mDA) neurons are also sensitive to spastizin and spatacsin levels. The identification of two causative genes in familial forms of Parkinson disease, PTEN-induced kinase 1 (PINK1) (21) and parkin (22), has provided strong evidence that dysregulation of mitochondrial degradation (mitophagy) are involved in Parkinson disease pathogenesis. Mitochondria are highly dynamic organelles that serve as the main source for cellular ATP, and mitochondrial dysfunction has been implicated in a wide variety of developmental and degenerative neurologic disorders. Neurons are highly dependent on mitochondria because of their limited glycolytic capacity (23). While there are only three HSP genes that encode clear mitochondrial proteins—paraplegin, C12orf65 and HSP60—there are some HSP subtypes associated with mitochondrial DNA mutations, and still others have evidence for mitochondrial trafficking disturbances. For instance, in SPG4 and SPG3A, decreased fast axonal transport of mitochondria has been observed (24–27).

Mitochondrial shape and size are intimately linked to their cellular distributions and are determined by a delicate balance between fusion and fission mechanoenzymes. Fusion-promoting proteins include the large GTPases mitofusin-1, mitofusin-2 and optic atrophy protein 1 (OPA1), while the dynamin-related protein 1 (DRP1) is the GTPase that mediates mitochondrial fission. Proper maintenance of mitochondrial morphology is very important for neuronal health, as a variety of neurodegenerative diseases are caused by mutations in genes encoding these fission/fusion proteins (28). Although spastizin has been shown to partially co-localize with mitochondria (7)—and spasticzin, spatacsin and AP-5 are all involved in lysosomal degradative processes—any contributions of these proteins to mitochondrial health have not been reported.

Advances in iPSC technology provide researchers a unique system to generate patient-specific neurons to study neurologic diseases (29–32). Over the past few years, iPSCs have been generated for three forms of HSP: SPG4, SPG3A and SPG11 (24,25,27,33). These patient-specific, iPSC-derived neurons recapitulate key disease-specific phenotypes, including impaired axonal transport of mitochondria (24,27). Here, we sought to examine the cellular pathogenesis of SPG15 and SPG48 using human pluripotent stem cells (hPSCs), including patient-specific induced pluripotent stem cells (iPSCs) and knockdown human embryonic stem cells (hESCs). We first generated SPG15 and SPG48 iPSCs and differentiated them into several neuronal lineages so that the effects of spastizin and AP5Z1 loss could be examined and compared across various types of human neurons which retain the patients' genetic backgrounds. This revealed cell-type specific defects in neurite projections, apoptosis, mitochondrial morphology and membrane potential. To further assess the potential role of mitochondria in HSP pathogenesis, control and HSP neurons were treated with mdivi-1, an inhibitor for DRP1. Application of mdivi-1 restored normal mitochondrial morphology and was effective at rescuing neurite outgrowth defects and late-onset apoptosis in SPG15 and SPG48 neurons. Moreover, direct knockdown of DRP1 using lentiviral shRNA rescued neurite outgrowth defects in SPG15 and SPG48 neurons, suggesting that mitochondrial dynamics are a potential therapeutic target for treating these HSPs.

Results

Generation and characterization of SPG15 and SPG48 iPSC lines

To generate iPSC lines, dermal fibroblasts from patients or control subjects (Supplementary Material, Fig. S1A) were transfected with episomal vectors containing Oct3/4, Klf4, L-Myc, Lin28 and Nanog (34). Emergent iPSC colonies were expanded for each group, and clones with typical ESC morphology were used for further analysis. The presence of mutations in the ZFYVE26 gene was confirmed by Sanger sequences in the iSPG15-1 lines (Supplementary Material, Fig. S1B). These mutations were not present in an unaffected sibling of the SPG15 patient, providing a control line that shares some genetic background. A homozygous premature stop codon in exon 15 of the AP5Z1 gene was confirmed in the iSPG48-1 iPSC line (Supplementary Material, Fig. S1C) (18). The SPG15 and SPG48 iPSC lines generated had typical hESC-like colony morphology (Supplementary Material, Fig. S1D) and expressed typical pluripotent stem cell markers, including Nanog, SSEA-4, and Tra-1-60 (Supplementary Material, Fig. S1E). Fibroblasts from the SPG15 patient and unaffected sibling were previously found to lack spastizin expression at the mRNA and protein levels (35). As expected, a significant reduction in ZFYVE26 and AP5Z1 mRNA transcript was observed in SPG15 and SPG48 iPSC-derived neurons, respectively (Supplementary Material, Fig. S2A and B).

Neurite outgrowth defects in SPG15 and SPG48 iPSC-derived neurons

To study the effects of spastizin and AP5Z1 depletion in clinically-relevant cell types, iPSC lines were differentiated to telencephalic glutamatergic neurons (36–38), spinal neurons (39,40) and mDA neurons (41) using well-established protocols. The differentiation efficiency was determined by examining the percentage of cells expressing markers for telencephalic glutamatergic neurons (Tbr1^{+}), spinal neurons (Hoxb4^{+}) and mDA neurons (tyrosine hydroxylase, TH[+]). No significant differences were observed between groups in generating these neuronal subtypes (Fig. 1A–D), suggesting that absence of these proteins does not affect neuronal specification. The ability of these neurons to project neurites was then examined and compared across neuronal subtypes (Fig. 1E–G). Interestingly, the length of the longest neurite, which generally develops into the axon,
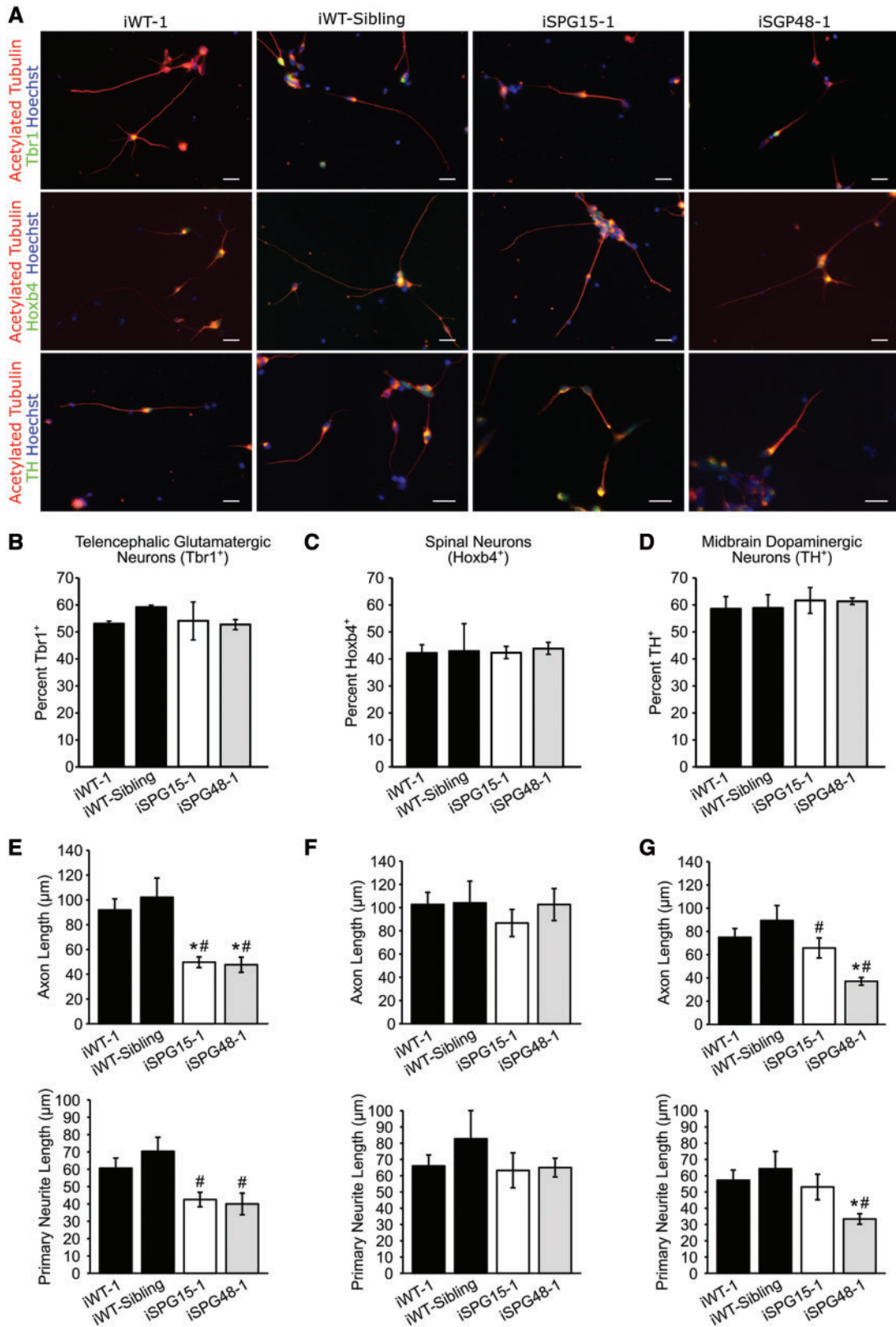
Figure 1. SPG15 and SPG48 neurons display impaired neurite outgrowth. (**A**) Immunofluorescence images of week 6 telencephalic, spinal and mDA neurons. Cells were stained for acetylated tubulin to label neurites, along with the telencephalic glutamatergic marker Tbr1, spinal neuron marker Hoxb4, or the dopaminergic marker TH. (**B**) Quantification of the percentage of Tbr1$^+$ neurons. (**C**) Quantification of Hoxb4$^+$ spinal neurons. (**D**) Quantification of TH$^+$ dopaminergic neurons. (**E**) Quantification of week 6 neurite outgrowth parameters, including average axon length (longest neurite) and average length of all primary neurites in Tbr1$^+$ neurons 48 h after plating. (**F**) Hoxb4$^+$ neurite outgrowth quantification. (**G**) TH$^+$ neurite outgrowth quantification. Data are presented as means $\pm$ SEM, $N = 3$–4 coverslips with a minimum of 50 cells analyzed per group. $^*P < 0.05$ compared with iWT-1; $^\#P < 0.05$ compared with iWT-sibling cells. Scale bars: 20 μm.
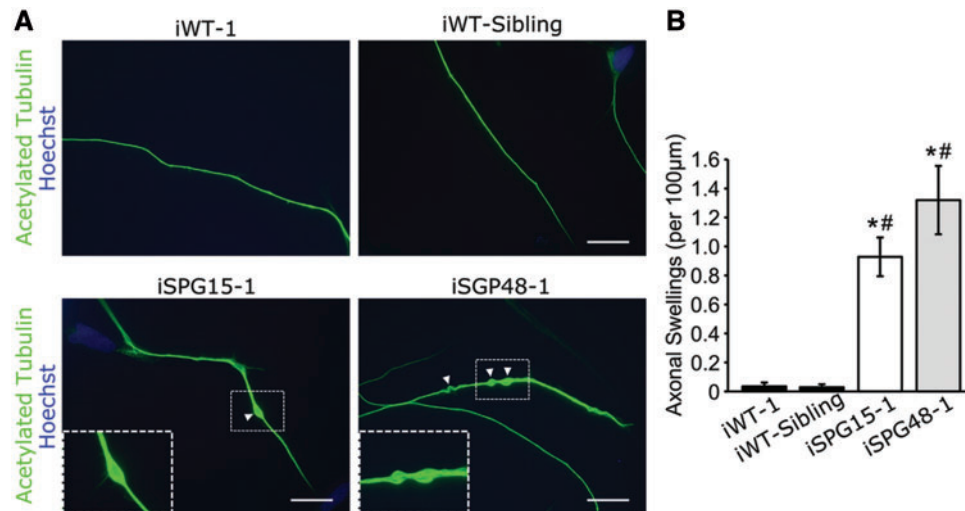
Figure 2. Increased neurite swellings within SPG15 and SPG48 telencephalic neurons. (**A**) Representative images of telencephalic neurons with axonal swellings labeled with arrowheads. Boxed regions are enlarged in the insets. Scale bars: 20 μm. (**B**) Quantification revealed a significant increase in axonal swellings in patient-derived neurons compared with control neurons. Data are presented as means ± SEM from at least 30 cells in three independent experiments. *$P < 0.05$ compared with iWT-1. #$P < 0.05$ compared with iWT-sibling cells.

was significantly reduced in SPG15 and SPG48 Tbr1^{+} and TH^{+} neurons, but not in Hoxb4^{+} neurons. The average length of primary neurites was also reduced in Tbr1^{+} SPG15 and SPG48 telencephalic neurons as well as in TH[+] SPG48 mDA neurons. Analysis of neurite outgrowth was repeated on additional clones, and SPG15 and SPG48 neurons again had reduced outgrowth in telencephalic glutamatergic neuron cultures (Supplementary Material, Fig. S3). These data suggest that neurite outgrowth in telencephalic and mDA neurons is sensitive to levels of spastizin and AP5Z1, while spinal neurons are not.

A hallmark pathologic change described in models of various HSP subtypes is the presence of enlarged, swollen axons (24,26,42,43). To examine whether such swellings are present, week 6 telencephalic glutamatergic neurons derived from SPG15 and SPG48 iPSCs were stained for acetylated tubulin. While there were almost no swellings in control lines, there was a significant increase in the number of swellings in SPG15 and SPG48 neurons, recapitulating disease-specific axonal defects (Fig. 2A and B).

Loss of spastizin and AP5Z1 alters mitochondrial morphology and function

Previously, it has been reported that spastizin partially localizes to mitochondria (7); therefore, we examined mitochondrial morphology in the affected neuronal subtypes. Telencephalic glutamatergic and mDA neuron cultures were stained with MitoTracker CMXRos to visualize mitochondria, and live-cell images were taken of primary neurites. This revealed a significant reduction in average mitochondrial length in SPG15 and SPG48 telencephalic glutamatergic neurons (Fig. 3A and B). There was also a reduction in aspect ratio (length/width) in the SPG15 neurons (Fig. 3C). In addition to this size change, there was a significant reduction in the number of mitochondria per 1 μm neurite for the SPG48 neurons (Fig. 3D) as well as a reduction in linear density for both groups (Fig. 3E). Neurons in the mDA cultures also showed changes to mitochondrial morphology. While mitochondrial length and aspect ratio were only altered in the SPG15 neurons (Fig. 3G and H), number and density of mitochondria along neurites were significantly reduced in both

SPG15 and SPG48 neurons (Fig. 3I and J). These results suggest that spastizin and AP5Z1 influence mitochondrial shape and distribution in neurons.

Next, we examined whether mitochondrial health was affected in SPG15 and SPG48 neurons. Cells were incubated with the fluorescent dye tetramethylrhodamine methyl ester (TMRM), which binds mitochondria based on their membrane potential ($\Delta\psi_m$) (44). This revealed a significant reduction in TMRM fluorescence in mitochondria of SPG15 telencephalic glutamatergic neurons (Fig. 4A and B). This TMRM signal was indeed dependent on $\Delta\psi_m$, as the uncoupler FCCP reduced TMRM fluorescence (Fig. 4C). Similarly, $\Delta\psi_m$ was significantly decreased in SPG48 telencephalic glutamatergic neurons as compared with control neurons (Fig. 4D). These data reveal that loss of spastizin or AP5Z1 has a negative effect on $\Delta\psi_m$, indicating reduced mitochondrial health in SPG15 and SPG48 neurons.

Inhibition of mitochondrial fission partially rescues SPG15 telencephalic neuron defects

Reduced sizes of mitochondria and increased apoptosis in SPG15 and SPG48 neurons suggested that these neurons might have increased mitochondrial fragmentation. We tested the effects of mdivi-1 (mitochondrial division inhibitor 1) in SPG15 and SPG48 neurons. This drug is an inhibitor of DRP1, which mediates mitochondrial fission (45). A concentration of 10 μM was chosen for mdivi-1, since it was previously reported to be effective in rescuing mitochondrial defects in mutant PINK1 dopaminergic neurons, without inducing the formation of donut-shaped mitochondria (46). Telencephalic glutamatergic neurons were plated onto coverslips, and 24 h later they were treated with 10 μM mdivi-1 or vehicle for another 48 h. Next, mitochondrial morphology and neurite outgrowth were examined. Treatment with mdivi-1 significantly rescued the reduction of mitochondrial numbers in both SPG15 and SPG48 neurons (Fig. 5A and B). While mdivi-1 paradoxically reduced the linear density of mitochondria in neurites of control neurons, albeit only modestly, it significantly increased linear density in SPG15 and SPG48 neurons (Fig. 5C). Decreases in average
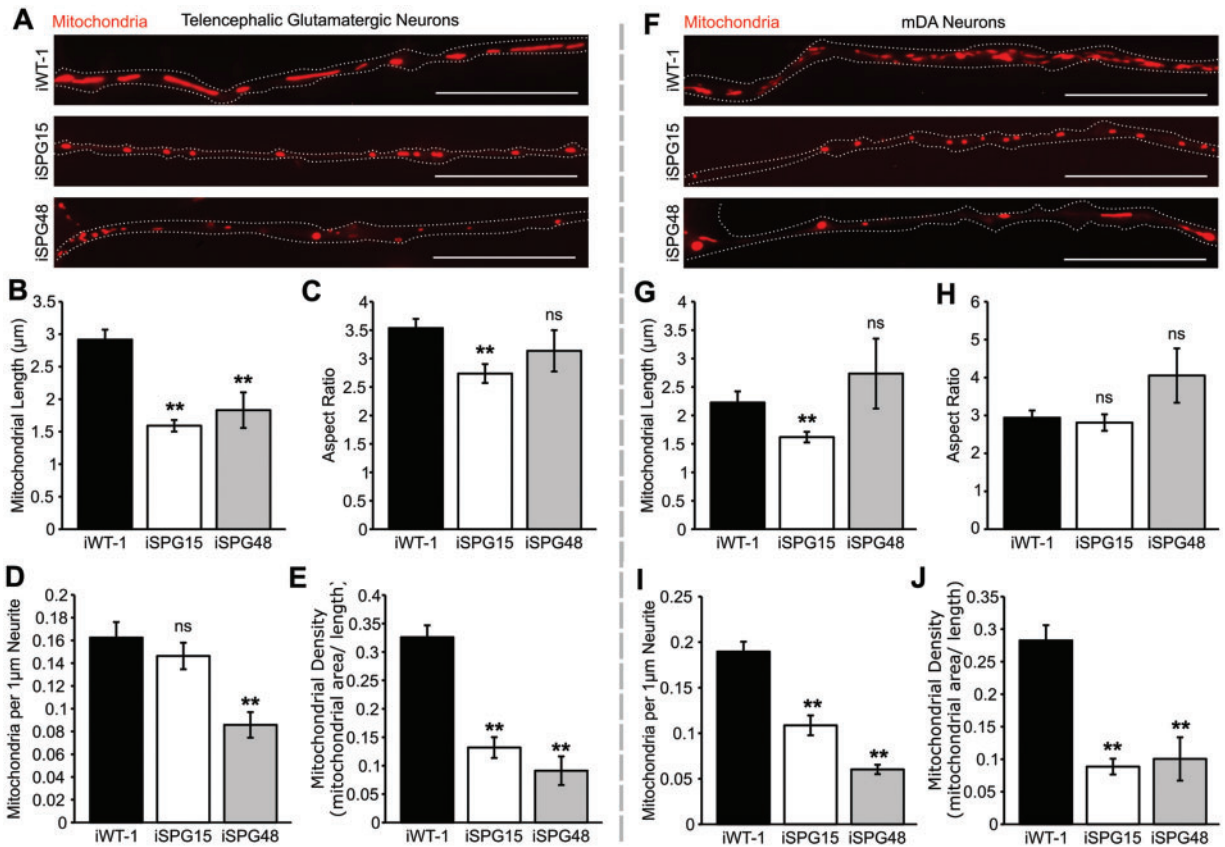
Figure 3. SPG15 and SPG48 neurons have altered mitochondrial morphology. (**A**) Immunofluorescence images of mitochondria within neurites taken in live, week 10 telencephalic glutamatergic neurons derived from iWT-1, iSPG15–1 and iSPG48–1 iPSCs, stained with MitoTracker CMXRos (red). (**B**) Average mitochondrial length, calculated by measuring the longest axis of each mitochondrion. (**C**) Average aspect ratio, calculated by dividing the major axis by the minor axis for each mitochondrion. (**D**) Average number of mitochondria per 1 μm neurite. (**E**) Average linear mitochondrial density, calculated by dividing the total mitochondrial area by the neurite length. (**F**) Mitochondrial staining in week 10 mDA neuron cultures derived from iWT-1, iSPG15-1 and iSPG48–1 iPSCs. (**G**) Mitochondrial length, (**H**) mitochondrial aspect ratio, (**I**) mitochondria per 1 μm neurite, and (**J**) linear mitochondrial density. Data are presented as means ± SEM from a minimal of 20 axon segments in three independent experiments. **$P < 0.01$ versus iWT-1; ns, not significant. Scale bars: 20 μm.

mitochondrial length were also rescued in SPG15 neurons, with a trend toward improvement in SPG48 neurons (Fig. 5D). Lastly, the aspect ratio was also increased in SPG15 neurons, and there was a non-significant trend towards an increase in SPG48 neurons (Fig. 5E). Together these results suggest that mdivi-1 may improve the health of mitochondria and thus increase their transport into neurites, since transport is reduced when mitochondria become damaged (47).

Next, we examined whether disease-specific axonal defects in SPG15 and SPG48 telencephalic neurons could be rescued after restoring mitochondrial morphology using mdivi-1. Neurite outgrowth was analyzed following 48 h of mdivi-1 treatment; primary neurite length in SPG15 and SPG48 neurons was significantly increased, to a level comparable to that of control neurons (Fig. 6A–C). Since alterations in mitochondrial membrane potential can result in release of cytochrome *c* from mitochondria and trigger apoptosis (48), we examined apoptosis in long-term SPG15 and SPG48 neurons using caspase 3/7 activity as a readout. Week 10 SPG15 neurons had significantly increased caspase 3/7 activity (Fig. 6D and E). Interestingly, mdivi-1 had no effect on caspase 3/7 activity in control neurons, but it caused a significant reduction in SPG15 and SPG48 telencephalic neurons (Fig. 6D and E). These findings suggest that restoring mitochondrial normal morphology can rescue the disease-specific phenotypes in SPG15 and SPG48 neurons.

Knocking down spastizin and AP5Z1 recapitulates phenotypes from SPG15 and SPG48 patient-derived neurons

To assess further the role of spastizin and AP5Z1 in neurite outgrowth and mitochondrial morphology, we generated spastizin- and AP5Z1-RNAi hESCs and differentiated these ESCs into telencephalic glutamatergic neurons. These cells were compared with H9 lines that expressed shRNAs which target luciferase (Luc RNAi), a gene not expressed in mammalian cells. Two shRNA constructs resulted in 51% and 52% knockdown of spastizin (Fig. 7A and B), and one shRNA targeting AP5Z1 resulted in 87% knockdown in H9 hESC-derived forebrain neurons (Fig. 7C). We then examined neurite outgrowth in spastizin- and AP5Z1-knockdown telencephalic neurons. Neurite outgrowth was significantly reduced in the knockdown neurons compared with controls, further supporting a role for spastizin and AP5Z1 in neurite development and maintenance (Fig. 7D–F). Interestingly, the neurite outgrowth defects in spastizin- and AP5Z1-knockdown neurons were also rescued following 48 h treatment with 10 μM mdivi-1 (Fig. 7D–F), recapitulating the effects seen in SPG15 and SPG48 iPSC-derived neurons. Together, these data suggest that loss of spastizin and AP5Z1 in SPG15 and SPG48 neurons, respectively, alters mitochondrial dynamics, leading to mitochondrial fragmentation and subsequent axonal defects.
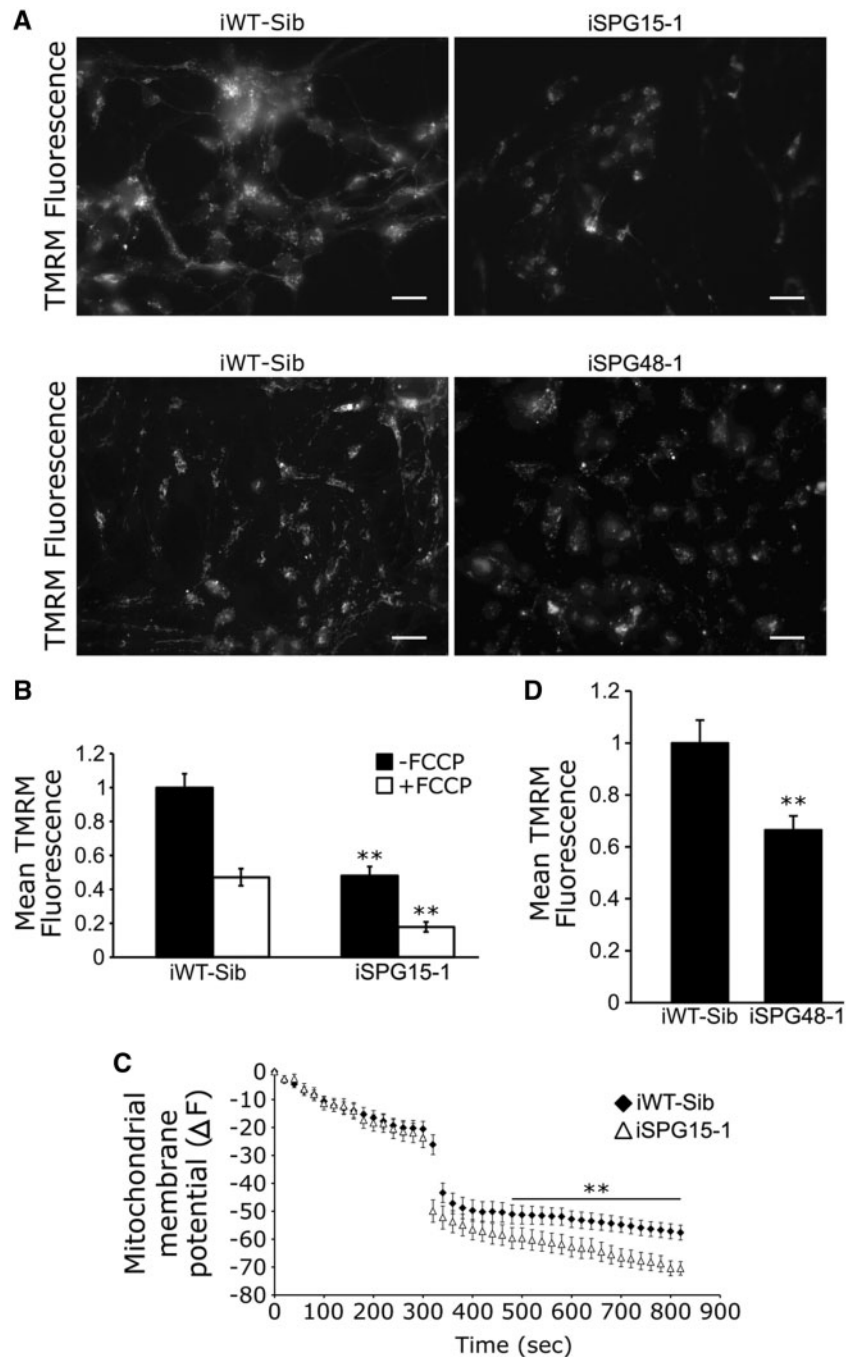
Figure 4. Reduced mitochondrial membrane potential in SPG15 and SPG48 neurons. (**A**) Representative images of control and SPG15 neurons stained with TMRM. Scale bars: 20 μm. (**B**) Quantification of average pixel fluorescence intensity of TMRM before and after FCCP treatment. (**C**) Changes in TMRM fluorescence intensity shown by ΔF, which represents the levels of mitochondrial membrane potential. FCCP was added at 300 s to decrease mitochondrial membrane potential. (**D**) TMRM fluorescence intensity was significantly decreased in SPG48 telencephalic neurons as compared with neurons derived from sibling control iPSCs. Data represent means ± SEM from at least 50 cells, in three independent experiments. **$P < 0.01$ versus iWT control.

Role of DRP1 in axonal defects of SPG15 and SPG48 neurons

Since mdivi-1 has also been reported to inhibit mitochondrial complex I (49), and we observed an unexpected shortening of mitochondrial length in control iPSC-derived neurons in response to mdivi-1 treatment, we generated lentivirus containing specific DRP1 shRNAs to more firmly establish the specific role of DRP1 (Fig. 8A). Lentiviruses containing shRNA targeting

luciferase were used as controls. We infected SPG15 and SPG48 telencephalic neurons with lentiviruses containing DRP1 shRNA (shRNA-b), which efficiently knocked down DRP1 expression in HEK293 cells (Fig. 8B), or else luciferase shRNA. The DRP1-shRNA-infected SPG15 and SPG48 neurons (as indicated by GFP expression) showed a dramatic recovery of their neurite outgrowth (Fig. 8C). Further quantification revealed that knockdown of Drp1 in SPG15 and SPG48 neurons significantly
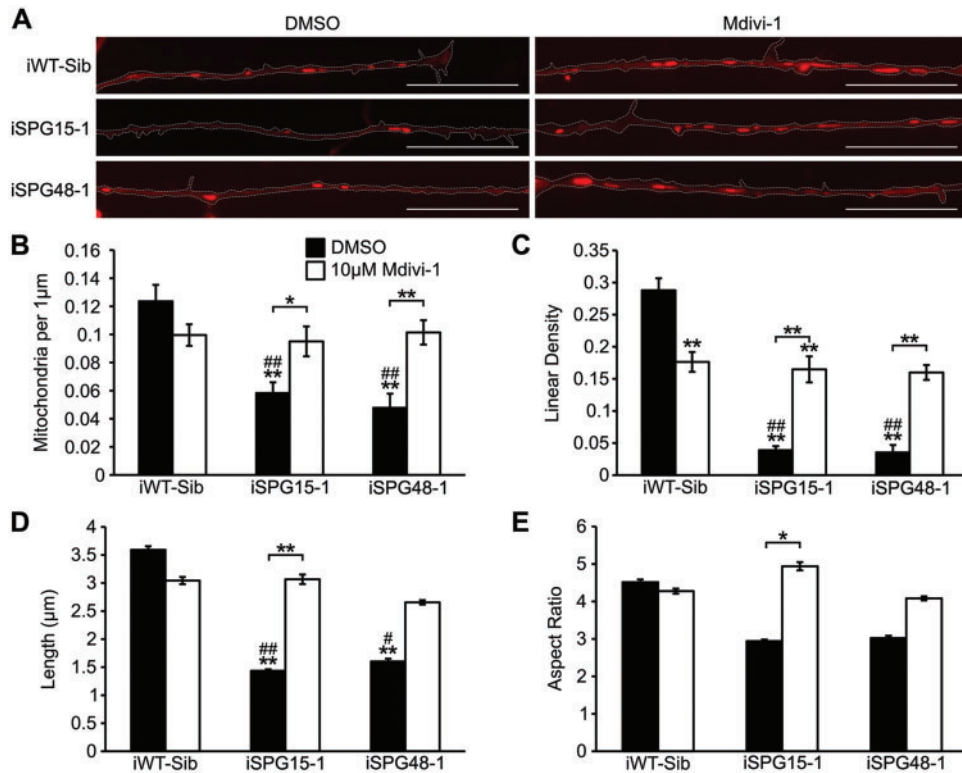
Figure 5. Inhibition of mitochondrial fission rescues mitochondrial morphology. (**A**) Representative image of axonal mitochondria stained with MitoTracker CMXRos (red) in cells treated with vehicle or 10 μM mdivi-1 for 48 h. (**B**) Quantification of the number of mitochondria per 1 μm axon. (**C**) Linear mitochondrial density. (**D**) Average mitochondrial length along axons. (**E**) Average mitochondrial aspect ratio. Data are presented as means ± SEM from at least 20 axon segments in three independent experiments. $^*P < 0.05$, $^{**}P < 0.01$ versus iWT-Sib DMSO treated. $^\#P < 0.05$, $^{\#\#}P < 0.01$ versus iWT-Sib, Mdivi-1-treated.

increased axonal length and primary neurite length of these neurons compared with control RNAi-treated SPG15 and SPG48 neurons, respectively (Fig. 8D and E). Together, these data demonstrate that neurite outgrowth deficits in SPG15 and SPG48 neurons can be rescued by direct downregulation of Drp1.

Discussion

Here, we have established human neuronal models for SPG15 and SPG48 by generating patient-specific iPSCs and differentiating these stem cells into different neuronal subtypes. Our results show that the lack of spastizin or AP5Z1 results in cell-type specific defects in telencephalic and mDA neurons but not in spinal neurons. Our data also implicate dysfunctional mitochondria in the pathogenesis of SPG15 and SPG48. There was a significant reduction in mitochondrial length and density within neurites, and these neurons had reduced $\Delta\psi_m$. Interestingly, treatment with the DRP1 inhibitor mdivi-1 rescued the mitochondrial morphology defects, partially rescued neurite outgrowth defects, and reduced caspase 3/7 activity in SPG15 and SPG48 neurons. The role of DRP1 in these HSPs was further supported by the rescue of neurite outgrowth deficits in these neurons after directly knocking down expression of DRP1. Thus, this study identifies a novel role of impaired mitochondrial morphology in the disease-specific phenotypes in SPG15 and SPG48 and provides a potential therapeutic strategy through targeting mitochondrial dynamics for these HSPs.

Both SPG15 and SPG48 telencephalic neurons exhibited a dramatic reduction in axon length and primary neurite length, while there was a more dramatic reduction in neurite

outgrowth parameters for SPG48 mDA neurons. Early neurite outgrowth defects appear to be a common finding among several HSP subtypes, including SPG3A (27), SPG4 (24) and SPG11 (33). Previous findings that both patient-specific SPG11 iPSC-derived cortical neurons and spatacsin knockdown neurons have reduced axonal outgrowth is significant, since this HSP subtype is nearly clinically identical to SPG15. The thin corpus callosum that is often associated with SPG15 and SPG11 is thought to be a developmental defect (50), which may arise from the reduced ability of corticofugal axons to reach their target. However, it is less clear whether this is a consistent feature of SPG48. In addition to iPSCs, we generated spastizin- and AP5Z1-knockdown hESCs, from which neurons were generated and exhibited similar phenotypes as patient iPSC-derived neurons. Since HSP is a relatively rare group of disorders, these HSP gene knockdown hESC lines can serve as unique models to confirm the findings obtained from iPSCs.

Spastizin was previously shown to partially co-localize with mitochondria (7). We found that SPG15 and SPG48 cells had smaller, fragmented mitochondria with a lower density along neurites. This suggests that spastizin levels may affect the mitochondrial fission/fusion balance. While it is possible that spastizin does so directly, it is more likely a secondary result of the reduced autophagic flux that occurs when spastizin and AP5Z1 levels are reduced (9,11,51), or secondary to endolysosomal defects more generally. Importantly, spastizin is important for autophagic lysosome reformation, a process that generates new free lysosomes (9). A deficiency in autophagic flux could result in the accumulation of autophagic material, including damaged mitochondria. We observed a decrease in mitochondrial
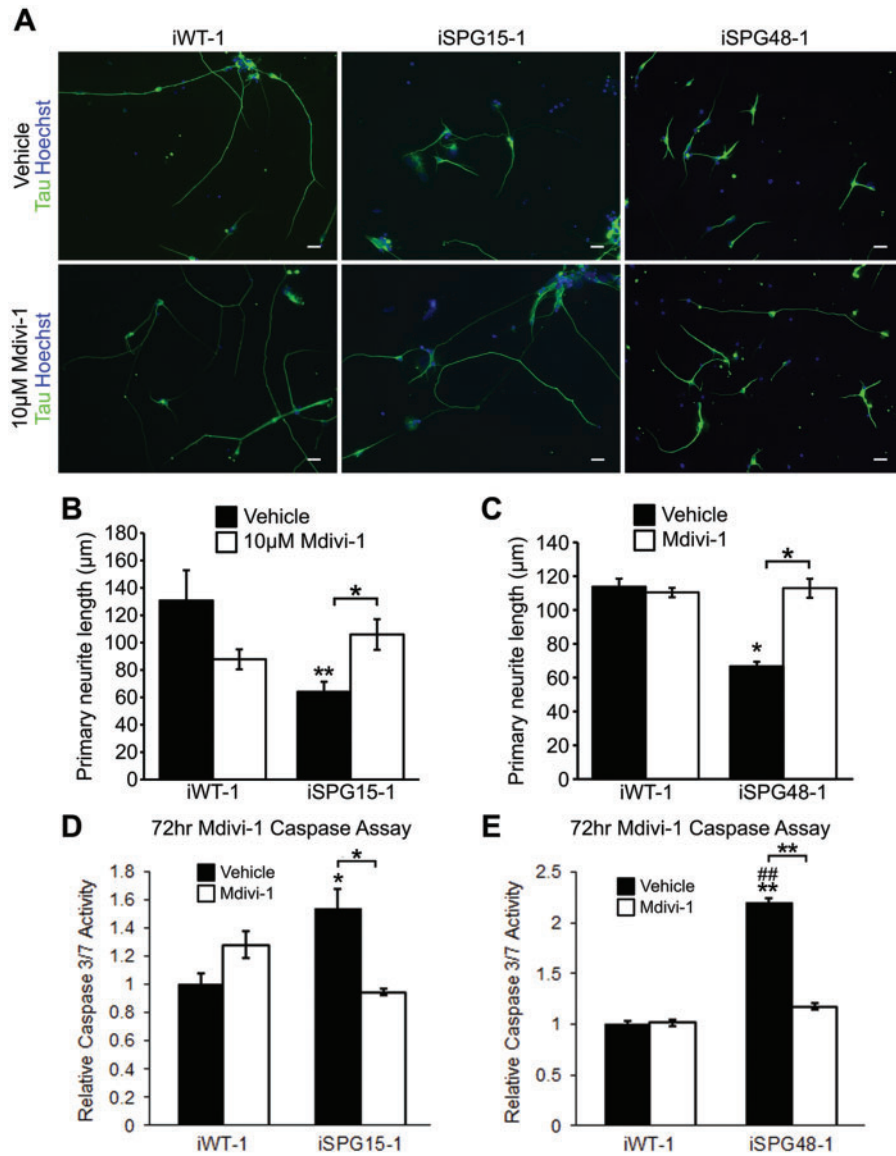
Figure 6. Inhibiting mitochondrial fission improves neurite outgrowth in SPG15 and SPG48 forebrain cells. (**A**) Representative images of telencephalic neurons following 48 h treatment with vehicle or 10 μM Mdivi-1. Scale bars: 20 μm. (**B, C**) Average length of the longest neurite in SPG15 (B) and SPG48 (C) cultures. (**D, E**) Caspase 3/7 activity in long-term SPG15 (D) or SPG48 (E) neurons following 72 h treatment with vehicle or Mdivi-1. Data are presented as means ± SEM from at least 30 cells in three independent experiments. $^*P < 0.05$, $^{**}P < 0.01$ versus iWT-1 Vehicle (DMSO)-treated group. $^{##}P < 0.01$ versus iWT-1, Mdivi-1-treated group.

$\Delta\psi_m$ and increased mitochondrial fragmentation, which resembles findings from familial forms of Parkinson disease, where PINK1 or parkin are mutated (46).

The Parkinson disease-associated proteins PINK1 and parkin are directly involved in mitophagy, a form of selective autophagy. Parkin is targeted to damaged mitochondria, such as those with low membrane potential, in a PINK1-dependent manner (52). Parkin then ubiquitinates mitochondrial proteins, allowing adaptor proteins such as p62 to bind and trigger phagophore formation, leading to degradation (53). The fragmented mitochondria observed in SPG15 and SPG48 neurons may be awaiting degradation via mitophagy, as mitochondrial fission has been shown to precede mitophagy (54,55). In the future, it will be interesting to further investigate the connection between spastizin, spatacsin, PINK1 and parkin, particularly since SPG15 and SPG11 are notable for early-onset parkinsonism in many cases. Our findings that the DRP1 inhibitor mdivi-1 as well as direct shRNA-mediated DRP1 depletion can partially rescue axon defects and reduce subsequent caspase-3/7 activity in SPG15 and SPG48 telencephalic neurons suggests that abnormal mitochondrial fragmentation is involved in the pathogenesis of these forms of HSP. Our results are reminiscent of a study where mitochondrial defects in mutant PINK1 N27 neuronal cells could also be rescued by the application of 10 μM mdivi-1 (46).

Regulation of mitochondrial fission and fusion is important during apoptosis (56), and though mitochondrial fusion is generally anti-apoptotic (57–59) while fission can be pro-apoptotic (45), a proper balance is critical. Indeed, neurologic syndrome are known with mutations in both mitochondrial fusion and fission GTPases (60,61). During apoptosis, DRP1 accumulates on mitochondria and increases the rate of division (45), and inhibition of DRP1 with mdivi-1 can reduce cytochrome c release following apoptosis stimulation. Even so, inhibition of DRP1
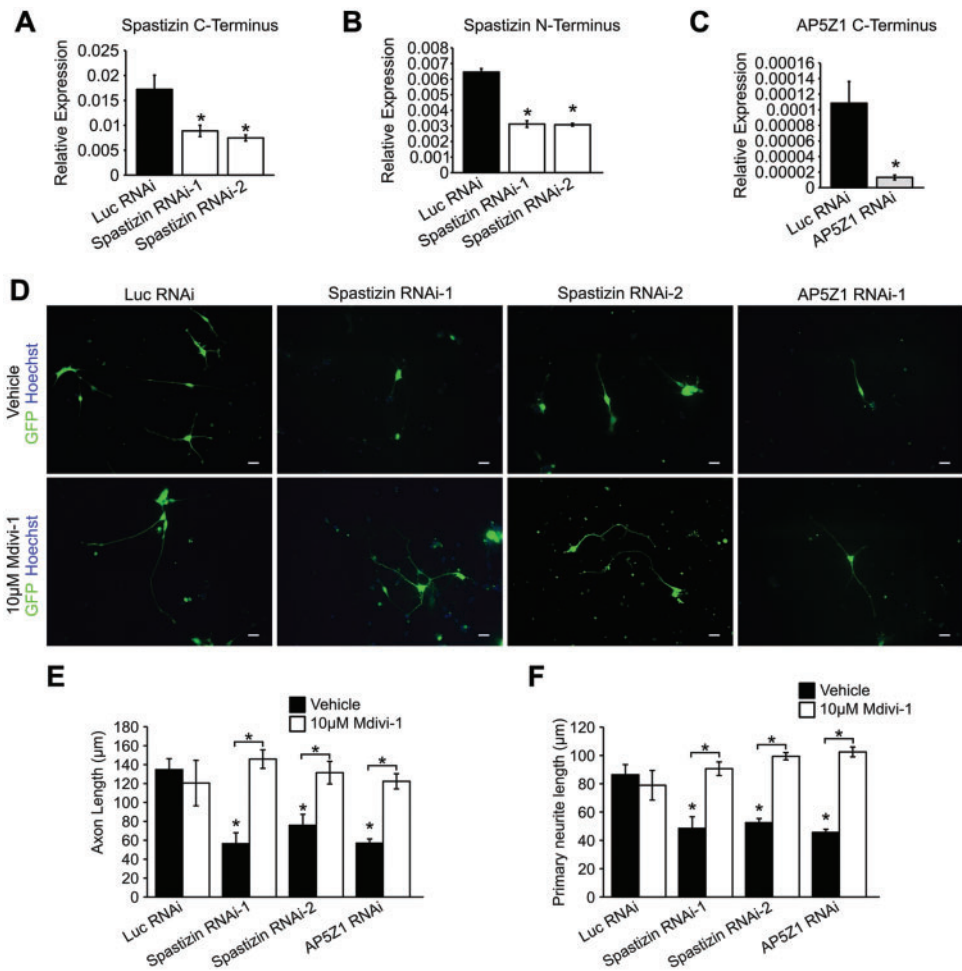
Figure 7. Knockdown of spastin and AP5Z1 recapitulates neurite outgrowth defects. (**A–C**) qRT-PCR expression of the C-terminus of spastizin transcript (A), N-terminus of spastizin transcript (B), or C-terminus of AP5Z1 transcript (C). (**D**) Representative images of week 6 knockdown forebrain neurons following 48 h treatment with vehicle or 10 μM mdivi-1. Scale bars: 20 μm. (**E**) Quantification of axon length in week 6 neurons. (**F**) Primary neurite length in week 6 neurons. Data are presented as means ± SEM from a minimum of 30 cells in three independent experiments. *$P < 0.05$ versus Luc RNAi or vehicle-treated groups.

function through hyperphosphorylation of Ser637 has been described in cells from patients with SPG31 (62), an autosomal dominant HSP whose gene product is linked most directly to regulation of ER morphology and cytoskeletal interactions. The models established here provide a powerful system to test mechanisms by which targeting mitochondrial fission/fusion improves neurite outgrowth and rescues axonal degeneration in different HSPs. In future studies, it will be particularly interesting to compare SPG15 and SPG48 iPSC-derived neurons with those from other HSPs such as SPG31, in order to clarify mechanisms underlying mitochondrial abnormalities in these HSPs.

Materials and Methods

Clinical studies

All study procedures were performed under an Institutional Review Board-approved clinical research protocol (NINDS protocol 00-N-0043) at the National Institutes of Health Clinical Center. The SPG15 patient is a 26-year-old woman who developed spastic paraparesis at around the age of 20. In addition, she has developed dysarthria, cognitive decline, fine action tremor and she is no longer able to work. Magnetic resonance imaging (MRI) identified significant thinning of the corpus

callosum (35). The SPG48 patient is a man in early 70s who developed symptoms of neuropathy, spastic paraplegia, ataxia, retinopathy and parkinsonism at about the age of 60 (63).

Reprogramming fibroblasts into iPSC lines

Human fibroblast cell lines were established from skin punch biopsies and maintained using standard procedures. To generate iPSC lines using episomal transduction, ~200 000 cells were dissociated and transfected with episomal plasmids (Addgene) containing pluripotency factors (Oct3/4, Sox2, L-Myc, Klf4 and Lin 28), as reported previously (34). At around 1 week after electroporation transduction, cells were plated onto a 35-mm dish in DMEM supplemented with 10% fetal bovine serum. After culturing for 7 days, cells were dissociated and seeded onto a mouse embryonic fibroblast (MEF) feeder at ~10^5 cells per 100 mm dish. Two weeks later, colonies with morphologies similar to hESCs were observed. These colonies were split onto MEF feeder cells to derive iPSC lines. After several passages, homogenous colonies with ESC-like morphology were generated and subjected for characterization. Control iPSC lines were also generated from a normal sibling (iWT-Sib) of the SPG15 patient (35) and a normal individual (iWT) as previously described (27).
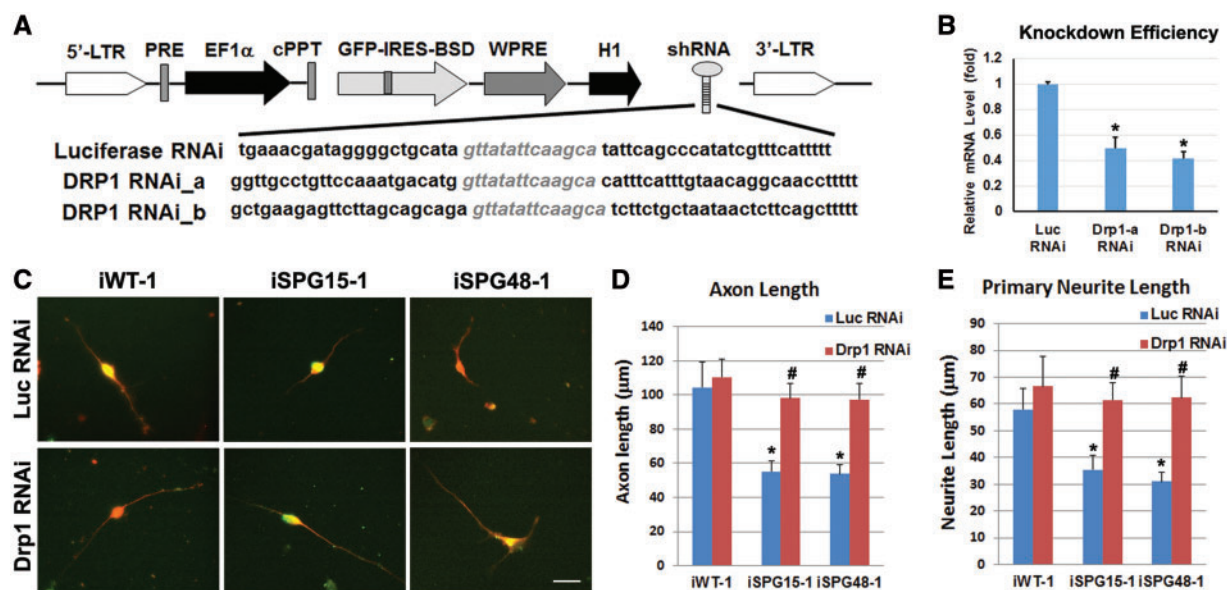
Figure 8. Effect of Drp1 knockdown in rescuing axonal defects in SPG15 and SPG48 iPSC-derived telencephalic neurons. (**A**) Schematic map of pLVTHM containing shRNAs that target Drp1. (**B**) To assess knockdown efficiency, HEK293 cells were transiently transfected with vectors expressing luciferase shRNA or Drp1 shRNAs. qRT-PCR analysis showed a significant reduction of Drp1 mRNA by both Drp1 shRNAs. (**C**) After Infection of Drp1 or Luciferase (Luc) RNAi viruses (GFP$^+$, green), Tau$^+$ (red) axons in telencephalic neurons from control, SPG15 and SPG48 groups were visualized. Scale bar: 20 μm. (**D, E**) There was a significant decrease in axonal length (**D**) and primary neurite length (**E**) in SPG15 and SPG48 neurons as compared with control neurons, which could be rescued by knocking down Drp1. Data are presented as means ± SEM from at least 15 axon segments in three independent experiments. *$P < 0.05$ versus Luc RNAi or iWT-1 control, #$P < 0.05$ versus iSPG15-1 or iSPG48-1 Luc RNAi.

The iPSC lines used in this study were iWT-1, iWT-2, iWT-Sib, iSPG15-1, iSPG15-2, iSPG48-1 and iSPG48-2 (Supplementary Material, Table S1).

Lentivirus production and transduction of hESCs

To knock down spastizin, AP5Z1 and Drp1, shRNAs were cloned into pLVTHM. To produce high-titer lentivirus, 10 μg of pLVTHM-shRNA lentiviral transfer vector, 7.5 μg of lentiviral vector psPAX2, and 5 μg of pMD2.G (VSV-G envelope protein) were cotransfected to HEK293FT cells (Invitrogen) using the calcium phosphate method. Sixty hours after transfection, cell culture medium containing viral particles were collected and filtered through a 0.45-μm filter (Millipore). The viral particles were further concentrated by ultracentrifugation (SW 28 rotor, Beckman) at 50 000g for 2 h. The pellet was resuspended in hESC medium (for spastizin and AP5Z1) or DMEM-F12 medium (for DRP1). For transduction with spastizin- and AP5Z1- shRNA, hESCs were passaged normally and pelleted by brief centrifugation. Cell pellets were then incubated with 100 μl of concentrated virus (10^6 transducing units/ml) at 37°C for 30 min. The virus and cell mixture was then transferred to a MEF feeder layer overnight, and the medium was changed the next day. Puromycin was used to select transfected cells, and knockdown hESC lines were expanded and then differentiated into telencephalic progenitors as described below. For infection of Drp1 shRNA lentiviruses, 10 μl of concentrated virus were added to cultured forebrain neurons (10 μl to one well of a 24-well plate); the medium was changed the next day, and the neurite outgrowth of these cultures was analyzed 2 days later.

Human iPSC forebrain neuron differentiation

To generate telencephalic neurons from iPSCs, stem cells were cultured on a feeder layer of irradiated MEFs in 6-well tissue culture-treated plates for around 6 days, with the human ESC media (+10 ng/ml fibroblast growth factor [FGF]-2) changed daily. When nearly confluent, cells were detached from the feeder layer to initiate neural differentiation, as described previously (36–38). Briefly, iPSC aggregates were cultured in suspension for 4 days in human ESC media and then transferred to neural induction media (NIM). After an additional 3 days in suspension, iPSC aggregates were plated onto 6-well tissue culture plates in NIM with 10% fetal bovine serum. After 12 h, the media was replaced with fresh NIM. Media was then changed every other day until day 17, when the generated neuroepithelial (NE) cells were isolated. Mechanically isolated NE cells were cultured in suspension with NIM (+B27, +cAMP, +insulin-like growth factor 1 [IGF-1]) to generate neurospheres for at least 10 additional days. On about day 28, neurospheres were dissociated and plated onto polyornithine- and laminin-coated coverslips in neural differentiation media (NDM) containing N2, B27, ascorbic acid, cAMP, laminin, IGF-1, brain-derived neurotrophic factor and glial-derived neurotrophic factor. Half of the media was changed every other day for 6–12 weeks, depending on the analysis to be performed. For treatment of cells with mdivi-1, the media was replaced with standard neural differentiation media supplemented with 10 μM mdivi-1 (Sigma-Aldrich) dissolved in DMSO.

Spinal neuron differentiation

The procedure for generating NE cells and spinal motor neurons from hESCs and iPSCs was essentially the same as described (39,40,64). Briefly, hPSCs were induced to neural lineage by forming ESC aggregations and then culturing in neural medium. Early NE cells were formed around 8–10 days after differentiation from hPSCs, which exhibited columnar morphology and started to organize into a rosette-like structure. Human PSC-derived NE cells at day 10 were then treated with RA (0.1 μM) for

caudalization in a neural medium, which consisted of DMEM/F-12 medium, N2 supplement and heparin. One week later (day 17), the posteriorized NE cells were isolated. For specifying spinal motor neurons, these NE clusters were suspended in the same neural medium supplemented with B27, RA (0.1 μM) and purmorphamine (1 μM) for around 2 weeks. For terminal differentiation, the neural progenitor-enriched clusters were plated onto ornithine/laminin-coated coverslips in neurobasal medium (Invitrogen) supplemented with N2 and B27.

mDA neuron differentiation

mDA neurons were generated following a previously described protocol (41). In short, hPSCs were treated using a protocol similar to the telencephalic glutamatergic neuron differentiation, with the addition of several morphogens. From days 10–21, 3 μM CHIR99021 was included in the NIM. From days 12–23, 2 μM purmorphamine was added to the NIM. From days 21–35, 200 ng/ml FGF8 was included in the NIM and NDM. Lastly, starting on day 23 sonic hedgehog (SHH, 10 ng/ml) was included in the NIM and NDM.

Immunocytochemistry

Confocal immunofluorescence microscopy and immunostaining were performed as described previously (24,27,37). The percentage of TBR1$^+$, Hoxb4$^+$ and TH$^+$ cells among total cells (Hoechst) was determined by taking three randomly selected fields per coverslip and blindly counted using MetaMorph software as we described previously (27). Overlapping areas were imaged at 20× and stitched together using AxioVision software. Antibodies used in this study included: mouse monoclonal IgM anti-Tra-1-60 (Santa Cruz, 1: 50); goat polyclonal IgG anti-Nanog (R&D Systems, 1: 500); mouse monoclonal IgG$_3$ anti-SSEA-4 (Developmental Studies Hybridoma Bank, 1: 100); mouse IgG$_{2b}$ monoclonal anti-acetylated tubulin (Sigma-Aldrich, 1: 10 000); rabbit IgG anti-tau (Sigma-Aldrich, 1: 100); rabbit polyclonal anti-Tbr1 (Proteintech, 1: 1000); mouse monoclonal IgG βIII-tubulin (TuJ-1; Developmental Studies Hybridoma Bank, 1: 100); mouse monoclonal anti-β-tubulin (Sigma-Aldrich, 1: 2000), rabbit monoclonal anti-TH (Pel-Freez, 1: 400), rabbit monoclonal anti-Hoxb4 (Abcam, 1: 400).

Neurite outgrowth measurements

Axonal outgrowth was quantified using the NeuronJ plugin for ImageJ (65). Here the length of the longest process which also had the greatest tau intensity was measured. For the experiments in Figure 1, instead of anti-Tau (rabbit-IgG), anti-acetylated tubulin (mouse IgG) was used to stain axons (the longest one was selected), which allows double staining with antibodies against TH (rabbit IgG), Tbr1 (rabbit IgG) and Hoxb4 (rabbit IgG). A minimum of 50 cells were quantified per line from 3–4 coverslips.

Live-cell imaging

Neurospheres were plated onto polyornithine and laminin-coated 35 mm dishes (MatTek). At 8 weeks of total differentiation, the cells were stained with 50 nM MitoTracker Red CMXRos (Invitrogen) for 3 min to allow visualization of mitochondria, after which the media was replaced with fresh neural differentiation media. Live-cell imaging was performed using a Zeiss Axiovert 200M microscope equipped with an incubation chamber. The cells were kept at 37°C with 5% CO$_2$ while imaging. Axons identified according to morphological criteria (constant thin diameter, long neurites, no branching and direct emergence from the cell body) were imaged every 5 s for 5 min, yielding 60 frames. Quantifications were performed using a protocol described previously (24). In short, the location of each mitochondrion was manually selected using the Track Points function in MetaMorph, and parameters such as distance from cell body and velocity were recorded. A velocity threshold of 300 nm/s was used to select microtubule based transport events (66). To determine the percentage of motile mitochondria, the total number of mitochondria that were present along the imaged neurite was counted and those that changed position (velocity >300 nm/s) in at least three consecutive frames were considered motile.

Mitochondrial morphology

Neuronal cultures on glass bottom 35 mm dishes were stained with 25 nM MitoTracker CMXRos in neural differentiation media for 2 min at 37°C. The cells were washed twice with fresh NDM, and 2 ml NDM were added to the dish. Live-cell imaging was performed using a Zeiss Axiovert 200M microscope equipped with an incubation chamber. The cells were kept at 37°C with 5% CO$_2$ while imaging. Axons identified according to morphological criteria (constant thin diameter, long neurites, no branching and direct emergence from the cell body) were imaged using a Plan-Apochromat 63×/1.40 Oil DIC objective, with identical microscope settings for each group. The 16-bit gray-scale images were thresholded in ImageJ (NIH), and the particle analysis function was used to measure morphological characteristics.

Measurement of mitochondrial membrane potential

Mitochondrial membrane potential was measured based on a previous protocol (44), and the fluorescent dye tetramethylrhodamine methyl ester (TMRM, Invitrogen) was used because it accumulates in mitochondria based on $\Delta\psi_m$. Neurons were plated on 35 mm glass-bottomed dishes. They were washed three times with 5 mM K$^+$, 2 mM Ca^{2+} Tyrodes solution, then incubated with 10 nM TMRM in 2 ml Tyrodes solution for 45 min at room temperature in the dark. Live-cell imaging was performed using a Zeiss Axiovert 200M microscope equipped with an incubation chamber, using an EC Plan-Neofluar 40×/1.30 Oil DIC objective. Cells were kept at 37°C with 5% CO$_2$ while imaging. Microscope settings were optimized using control cells, and these same settings were used for all other groups. Randomly selected fields were imaged every 20 s for a total of 600 s. The mitochondrial uncoupler FCCP was added to the media after 300 s to a final concentration of 1 μM. Time series were analyzed in MetaMorph, and at least 20 regions of interest (ROIs) were traced around mitochondrial structures for each cell, along with adjacent background regions. The pixel intensity for each region was determined, followed by background subtraction. Changes in fluorescence were calculated with the formula $\Delta F = (F - F_0)/F_0 \times 100$, where F is the fluorescence intensity at any time point, and F_0 is the initial fluorescence.

Caspase 3/7 activity assay

For measurements of caspase 3 and 7 activities, the Caspase-Glo 3/7 Assay (Promega) was carried out according to the manufacturer's instructions. Briefly, motor neuron progenitor-enriched cultures were dissociated with Accutase (Invitrogen) and seeded onto 96-well plates at 5000 cells/well in 50 μl of caspase-3/7 reagent. After incubation for 1 h at room temperature, luminescence from each well was measured using a Wallac VICTOR2 1420 MultiLabel Counter.

Statistical analysis

The statistical significance of mean values among multiple sample groups was analyzed with Tukey's range test after ANOVA. Two-sided *t*-tests were used to examine the statistical significance between two sample groups. The significance level was defined as $P < 0.05$, and significance tests were conducted using SAS 9.1 (SAS Institute).

Supplementary Material

Supplementary Material is available at *HMG* online.

Acknowledgements

References

1. Blackstone, C., O'Kane, C.J. and Reid, E. (2011) Hereditary spastic paraplegias: membrane traffic and the motor pathway. *Nat. Rev. Neurosci.*, **12**, 31–42.

2. Novarino, G., Fenstermaker, A.G., Zaki, M.S., Hofree, M., Silhavy, J.L., Heiberg, A.D., Abdellateef, M., Rosti, B., Scott, E., Mansour, L. *et al.* (2014) Exome sequencing links corticospinal motor neuron disease to common neurodegenerative disorders. *Science*, **343**, 506–511.

3. Goizet, C., Boukhris, A., Maltete, D., Guyant-Marechal, L., Truchetto, J., Mundwiller, E., Hanein, S., Jonveaux, P., Roelens, F., Loureiro, J. *et al.* (2009) SPG15 is the second most common cause of hereditary spastic paraplegia with thin corpus callosum. *Neurology*, **73**, 1111–1119.

4. Pensato, V., Castellotti, B., Gellera, C., Pareyson, D., Ciano, C., Nanetti, L., Salsano, E., Piscosquito, G., Sarto, E., Eoli, M. *et al.* (2014) Overlapping phenotypes in complex spastic paraplegias SPG11, SPG15, SPG35 and SPG48. *Brain*, **137**, 1907–1920.

5. Hanein, S., Martin, E., Boukhris, A., Byrne, P., Goizet, C., Hamri, A., Benomar, A., Lossos, A., Denora, P., Fernandez, J. *et al.* (2008) Identification of the SPG15 gene, encoding spastizin, as a frequent cause of complicated autosomal-recessive spastic paraplegia, including Kjellin syndrome. *Am. J. Hum. Genet.*, **82**, 992–1002.

6. Schule, R., Schlipf, N., Synofzik, M., Klebe, S., Klimpe, S., Hehr, U., Winner, B., Lindig, T., Dotzer, A., Riess, O. *et al.* (2009) Frequency and phenotype of SPG11 and SPG15 in complicated hereditary spastic paraplegia. *J. Neurol. Neurosurg. Psychiatry*, **80**, 1402–1404.

7. Murmu, R.P., Martin, E., Rastetter, A., Esteves, T., Muriel, M.P., El Hachimi, K.H., Denora, P.S., Dauphin, A., Fernandez, J.C., Duyckaerts, C. *et al.* (2011) Cellular distribution and subcellular localization of spatacsin and spastizin, two proteins involved in hereditary spastic paraplegia. *Mol. Cell. Neurosci.*, **47**, 191–202.

8. Martin, E., Yanicostas, C., Rastetter, A., Alavi Naini, S.M., Maouedj, A., Kabashi, E., Rivaud-Pechoux, S., Brice, A., Stevanin, G. and Soussi-Yanicostas, N. (2012) Spatacsin and spastizin act in the same pathway required for proper spinal motor neuron axon outgrowth in zebrafish. *Neurobiol. Dis.*, **48**, 299–308.

9. Chang, J., Lee, S. and Blackstone, C. (2014) Spastic paraplegia proteins spastizin and spatacsin mediate autophagic lysosome reformation. *J. Clin. Invest.*, **124**, 5249–5262.

10. Vantaggiato, C., Clementi, E. and Bassi, M.T. (2014) ZFYVE26/SPASTIZIN: a close link between complicated hereditary spastic paraparesis and autophagy. *Autophagy*, **10**, 374–375.

11. Vantaggiato, C., Crimella, C., Airoldi, G., Polishchuk, R., Bonato, S., Brighina, E., Scarlato, M., Musumeci, O., Toscano, A., Martinuzzi, A. *et al.* (2013) Defective autophagy in spastizin mutated patients with hereditary spastic paraparesis type 15. *Brain*, **136**, 3119–3139.

12. Słabicki, M., Theis, M., Krastev, D.B., Samsonov, S., Mundwiller, E., Junqueira, M., Paszkowski-Rogacz, M., Teyra, J., Heninger, A.-K., Poser, I. *et al.* (2010) A genome-scale DNA repair RNAi screen identifies SPG48 as a novel gene associated with hereditary spastic paraplegia. *PLoS Biol.*, **8**, e1000408.

13. Hirst, J., Borner, G.H., Edgar, J., Hein, M.Y., Mann, M., Buchholz, F., Antrobus, R. and Robinson, M.S. (2013) Interaction between AP-5 and the hereditary spastic paraplegia proteins SPG11 and SPG15. *Mol. Biol. Cell*, **24**, 2558–2569.

14. Hirst, J., Irving, C. and Borner, G.H. (2013) Adaptor protein complexes AP-4 and AP-5: new players in endosomal trafficking and progressive spastic paraplegia. *Traffic*, **14**, 153–164.

15. Hirst, J., Barlow, L.D., Francisco, G.C., Sahlender, D.A., Seaman, M.N., Dacks, J.B. and Robinson, M.S. (2011) The fifth adaptor protein complex. *PLoS Biol.*, **9**, e1001170.

16. Branchu, J., Boutry, M., Sourd, L., Depp, M., Leone, C., Corriger, A., Vallucci, M., Esteves, T., Matusiak, R., Dumont, M. *et al.* (2017) Loss of spatacsin function alters lysosomal lipid clearance leading to upper and lower motor neuron degeneration. *Neurobiol. Dis.*, **102**, 21–37.

17. Khundadze, M., Kollmann, K., Koch, N., Biskup, C., Nietzsche, S., Zimmer, G., Hennings, J.C., Huebner, A.K., Symmank, J., Jahic, A. *et al.* (2013) A hereditary spastic paraplegia mouse model supports a role of ZFYVE26/SPASTIZIN for the endolysosomal system. *PLoS Genet.*, **9**, e1003988.

18. Hirst, J., Edgar, J.R., Esteves, T., Darios, F., Madeo, M., Chang, J., Roda, R.H., Dürr, A., Anheim, M., Gellera, C. *et al.* (2015) Loss of AP-5 results in accumulation of aberrant endolysosomes: defining a new type of lysosomal storage disease. *Hum. Mol. Genet.*, **24**, 4984–4996.

19. Guidubaldi, A., Piano, C., Santorelli, F.M., Silvestri, G., Petracca, M., Tessa, A. and Bentivoglio, A.R. (2011) Novel mutations in SPG11 cause hereditary spastic paraplegia associated with early-onset levodopa-responsive Parkinsonism. *Mov. Disord.*, **26**, 553–556.

20. Mallaret, M., Lagha-Boukbiza, O., Biskup, S., Namer, I.J., Rudolf, G., Anheim, M. and Tranchant, C. (2014) SPG15: a

cause of juvenile atypical levodopa responsive parkinson-ism. *J. Neurol.*, **261**, 435–437.

21. Valente, E.M., Abou-Sleiman, P.M., Caputo, V., Muqit, M.M., Harvey, K., Gispert, S., Ali, Z., Del Turco, D., Bentivoglio, A.R., Healy, D.G. *et al.* (2004) Hereditary early-onset Parkinson's disease caused by mutations in PINK1. *Science*, **304**, 1158–1160.

22. Kitada, T., Asakawa, S., Hattori, N., Matsumine, H., Yamamura, Y., Minoshima, S., Yokochi, M., Mizuno, Y. and Shimizu, N. (1998) Mutations in the parkin gene cause auto-somal recessive juvenile parkinsonism. *Nature*, **392**, 605–608.

23. DuBoff, B., Feany, M. and Gotz, J. (2013) Why size matters - balancing mitochondrial dynamics in Alzheimer's disease. *Trends Neurosci.*, **36**, 325–335.

24. Denton, K.R., Lei, L., Grenier, J., Rodionov, V., Blackstone, C. and Li, X.J. (2014) Loss of spastin function results in disease-specific axonal defects in human pluripotent stem cell-based models of hereditary spastic paraplegia. *Stem Cells*, **32**, 414–423.

25. Havlicek, S., Kohl, Z., Mishra, H.K., Prots, I., Eberhardt, E., Denguir, N., Wend, H., Plotz, S., Boyer, L., Marchetto, M.C. *et al.* (2014) Gene dosage-dependent rescue of HSP neurite defects in SPG4 patients' neurons. *Hum. Mol. Genet.*, **23**, 2527–2541.

26. Kasher, P.R., De Vos, K.J., Wharton, S.B., Manser, C., Bennett, E.J., Bingley, M., Wood, J.D., Milner, R., McDermott, C.J., Miller, C.C. *et al.* (2009) Direct evidence for axonal transport defects in a novel mouse model of mutant spastin-induced hereditary spastic paraplegia (HSP) and human HSP patients. *J. Neurochem.*, **110**, 34–44.

27. Zhu, P.-P., Denton, K.R., Pierson, T.M., Li, X.J. and Blackstone, C. (2014) Pharmacologic rescue of axon growth defects in a human iPSC model of hereditary spastic paraplegia SPG3A. *Hum. Mol. Genet.*, **23**, 5638–5648.

28. Burte, F., Carelli, V., Chinnery, P.F. and Yu-Wai-Man, P. (2015) Disturbed mitochondrial dynamics and neurodegen-erative disorders. *Nat. Rev. Neurol.*, **11**, 11–24.

29. Barral, S. and Kurian, M.A. (2016) Utility of induced pluripo-tent stem cells for the study and treatment of genetic dis-eases: focus on childhood neurological disorders. *Front. Mol. Neurosci.*, **9**, 78.

30. Chamberlain, S.J., Li, X.J. and Lalande, M. (2008) Induced plu-ripotent stem (iPS) cells as in vitro models of human neuro-genetic disorders. *Neurogenetics*, **9**, 227–235.

31. Dimos, J.T., Rodolfa, K.T., Niakan, K.K., Weisenthal, L.M., Mitsumoto, H., Chung, W., Croft, G.F., Saphier, G., Leibel, R., Goland, R. *et al.* (2008) Induced pluripotent stem cells gener-ated from patients with ALS can be differentiated into motor neurons. *Science*, **321**, 1218–1221.

32. Ito, D., Okano, H. and Suzuki, N. (2012) Accelerating progress in induced pluripotent stem cell research for neurological diseases. *Ann. Neurol.*, **72**, 167–174.

33. Perez-Branguli, F., Mishra, H.K., Prots, I., Havlicek, S., Kohl, Z., Saul, D., Rummel, C., Dorca-Arevalo, J., Regensburger, M., Graef, D. *et al.* (2014) Dysfunction of spatacsin leads to axonal pathology in SPG11-linked hereditary spastic paraplegia. *Hum. Mol. Genet.*, **23**, 4859–4874.

34. Okita, K., Matsumura, Y., Sato, Y., Okada, A., Morizane, A., Okamoto, S., Hong, H., Nakagawa, M., Tanabe, K., Tezuka, K. *et al.* (2011) A more efficient method to generate integration-free human iPS cells. *Nat. Methods*, **8**, 409–412.

35. Renvoisé, B., Chang, J., Singh, R., Yonekawa, S., FitzGibbon, E.J., Mankodi, A., Vanderver, A., Schindler, A., Toro, C., Gahl, W.A. *et al.* (2014) Lysosomal abnormalities in hereditary spastic paraplegia types SPG15 and SPG11. *Ann. Clin. Transl. Neurol.*, **1**, 379–389.

36. Boisvert, E.M., Denton, K., Lei, L. and Li, X.J. (2013) The specification of telencephalic glutamatergic neurons from human pluripotent stem cells. *J. Vis. Exp.*, **74**, e50321. doi: 10.3791/50321.

37. Li, X.J., Zhang, X., Johnson, M.A., Wang, Z.B., Lavaute, T. and Zhang, S.C. (2009) Coordination of sonic hedgehog and Wnt signaling determines ventral and dorsal telencephalic neu-ron types from human embryonic stem cells. *Development*, **136**, 4055–4063.

38. Zeng, H., Guo, M., Martins-Taylor, K., Wang, X., Zhang, Z., Park, J.W., Zhan, S., Kronenberg, M.S., Lichtler, A., Liu, H.X. *et al.* (2010) Specification of region-specific neurons including forebrain glutamatergic neurons from human induced plu-ripotent stem cells. *PLoS One*, **5**, e11853.

39. Li, X.J., Du, Z.W., Zarnowska, E.D., Pankratz, M., Hansen, L.O., Pearce, R.A. and Zhang, S.C. (2005) Specification of moto-neurons from human embryonic stem cells. *Nat. Biotechnol.*, **23**, 215–221.

40. Li, X.J., Hu, B.Y., Jones, S.A., Zhang, Y.S., Lavaute, T., Du, Z.W. and Zhang, S.C. (2008) Directed differentiation of ventral spi-nal progenitors and motor neurons from human embryonic stem cells by small molecules. *Stem Cells*, **26**, 886–893.

41. Xi, J., Liu, Y., Liu, H., Chen, H., Emborg, M.E. and Zhang, S.C. (2012) Specification of midbrain dopamine neurons from pri-mate pluripotent stem cells. *Stem Cells*, **30**, 1655–1663.

42. Fassier, C., Tarrade, A., Peris, L., Courageot, S., Mailly, P., Dalard, C., Delga, S., Roblot, N., Lefevre, J., Job, D. *et al.* (2013) Microtubule-targeting drugs rescue axonal swellings in cor-tical neurons from spastin knockout mice. *Dis. Model. Mech.*, **6**, 72–83.

43. Tarrade, A., Fassier, C., Courageot, S., Charvin, D., Vitte, J., Peris, L., Thorel, A., Mouisel, E., Fonknechten, N., Roblot, N. *et al.* (2006) A mutation of spastin is responsible for swellings and impairment of transport in a region of axon character-ized by changes in microtubule composition. *Hum. Mol. Genet.*, **15**, 3544–3558.

44. Joshi, D.C. and Bakowska, J.C. (2011) Determination of mito-chondrial membrane potential and reactive oxygen species in live rat cortical neurons. *J. Vis. Exp.*, **51**, e2704. doi: 10.3791/2704.

45. Cassidy-Stone, A., Chipuk, J.E., Ingerman, E., Song, C., Yoo, C., Kuwana, T., Kurth, M.J., Shaw, J.T., Hinshaw, J.E., Green, D.R. *et al.* (2008) Chemical inhibition of the mitochondrial di-vision dynamin reveals its role in Bax/Bak-dependent mito-chondrial outer membrane permeabilization. *Dev. Cell*, **14**, 193–204.

46. Cui, M., Tang, X., Christian, W.V., Yoon, Y. and Tieu, K. (2010) Perturbations in mitochondrial dynamics induced by hu-man mutant PINK1 can be rescued by the mitochondrial di-vision inhibitor mdivi-1. *J. Biol. Chem.*, **285**, 11740–11752.

47. Miller, K.E. and Sheetz, M.P. (2004) Axonal mitochondrial transport and potential are correlated. *J. Cell Sci.*, **117**, 2791–2804.

48. Gottlieb, E., Armour, S.M., Harris, M.H. and Thompson, C.B. (2003) Mitochondrial membrane potential regulates matrix configuration and cytochrome c release during apoptosis. *Cell Death Differ.*, **10**, 709–717.

49. Bordt, E.A., Clerc, P., Roelofs, B.A., Saladino, A.J., Tretter, L., Adam-Vizi, V., Cherok, E., Khalil, A., Yadava, N., Ge, S.X. *et al.* (2017) The putative Drp1 inhibitor mdivi-1 is a reversible mi-tochondrial complex I inhibitor that modulates reactive oxy-gen species. *Dev. Cell*, **40**, 583–594. e586.

50. Fink, J.K. (2013) Hereditary spastic paraplegia: clinico-pathologic features and emerging molecular mechanisms. *Acta Neuropathol.*, **126**, 307–328.

51. Sagona, A.P., Nezis, I.P., Bache, K.G., Haglund, K., Bakken, A.C., Skotheim, R.I. and Stenmark, H. (2011) A tumor-associated mutation of FYVE-CENT prevents its interaction with Beclin 1 and interferes with cytokinesis. *PLoS One*, **6**, e17086.

52. Narendra, D., Tanaka, A., Suen, D.F. and Youle, R.J. (2008) Parkin is recruited selectively to impaired mitochondria and promotes their autophagy. *J. Cell Biol.*, **183**, 795–803.

53. Exner, N., Lutz, A.K., Haass, C. and Winklhofer, K.F. (2012) Mitochondrial dysfunction in Parkinson's disease: molecular mechanisms and pathophysiological consequences. *EMBO J.*, **31**, 3038–3062.

54. Tanaka, A., Cleland, M.M., Xu, S., Narendra, D.P., Suen, D.F., Karbowski, M. and Youle, R.J. (2010) Proteasome and p97 mediate mitophagy and degradation of mitofusins induced by Parkin. *J. Cell Biol.*, **191**, 1367–1380.

55. Twig, G., Elorza, A., Molina, A.J., Mohamed, H., Wikstrom, J.D., Walzer, G., Stiles, L., Haigh, S.E., Katz, S., Las, G. *et al.* (2008) Fission and selective fusion govern mitochondrial segregation and elimination by autophagy. *EMBO J.*, **27**, 433–446.

56. Youle, R.J. (2005) Morphology of mitochondria during apoptosis: worms-to-beetles in worms. *Dev. Cell*, **8**, 298–299.

57. Neuspiel, M., Zunino, R., Gangaraju, S., Rippstein, P. and McBride, H. (2005) Activated mitofusin 2 signals mitochondrial fusion, interferes with Bax activation, and reduces susceptibility to radical induced depolarization. *J. Biol. Chem.*, **280**, 25060–25070.

58. Olichon, A., Baricault, L., Gas, N., Guillou, E., Valette, A., Belenguer, P. and Lenaers, G. (2003) Loss of OPA1 perturbates the mitochondrial inner membrane structure and integrity, leading to cytochrome c release and apoptosis. *J. Biol. Chem.*, **278**, 7743–7746.

59. Sugioka, R., Shimizu, S. and Tsujimoto, Y. (2004) Fzo1, a protein involved in mitochondrial fusion, inhibits apoptosis. *J. Biol. Chem.*, **279**, 52726–52734.

60. Archer, S.L. (2013) Mitochondrial dynamics–mitochondrial fission and fusion in human diseases. *N. Engl. J. Med.*, **369**, 2236–2251.

61. Westermann, B. (2010) Mitochondrial fusion and fission in cell life and death. *Nat. Rev. Mol. Cell. Biol.*, **11**, 872–884.

62. Lavie, J., Serrat, R., Bellance, N., Courtand, G., Dupuy, J.W., Tesson, C., Coupry, I., Brice, A., Lacombe, D., Durr, A. *et al.* (2017) Mitochondrial morphology and cellular distribution are altered in SPG31 patients and are linked to DRP1 hyperphosphorylation. *Hum. Mol. Genet.*, **26**, 674–685.

63. Hirst, J., Madeo, M., Smets, K., Edgar, J.R., Schols, L., Li, J., Yarrow, A., Deconinck, T., Baets, J., Van Aken, E. *et al.* (2016) Complicated spastic paraplegia in patients with AP5Z1 mutations (SPG48). *Neurol. Genet.*, **2**, e98.

64. Zhang, S.C., Wernig, M., Duncan, I.D., Brustle, O. and Thomson, J.A. (2001) In vitro differentiation of transplantable neural precursors from human embryonic stem cells. *Nat. Biotechnol.*, **19**, 1129–1133.

65. Schneider, C.A., Rasband, W.S. and Eliceiri, K.W. (2012) NIH Image to ImageJ: 25 years of image analysis. *Nat. Methods*, **9**, 671–675.

66. De Vos, K.J. and Sheetz, M.P. (2007) Visualization and quantification of mitochondrial dynamics in living animal cells. *Methods Cell. Biol.*, **80**, 627–682.